Proceedings of the 19th International Conference on Automation & Computing, Brunel University, London, UK, 13-14 September 2013

Dispersion Behavior of Torsional Guided Waves in a Small Diameter Steel Gas Pipe

Bahareh Zaghari[1], Victor Humphrey, Mohamed Moshrefi-Torbati
Institute of Sound and Vibration Research, University of Southampton
Southampton SO17 1BJ, UK
[1]b.zaghari@soton.ac.uk

***Abstract*— Condition monitoring of gas pipes has been an important issue for gas companies. Failure to accurately identify condition of gas pipes result in numerous problems. Also, producing a condition monitoring system for buried pipelines is challenging. Small pipes (with diameters less than 50 mm) are considered here as most of the literature focuses on larger pipes. Guided wave theory will be introduced alongside a numerical simulation of the relevant dispersion curves of the system. This paper investigates the feasibility of using torsional guided waves for inspecting defects in buried pipes with small diameters. The pipes are assumed to be lossless and hence the effect of attenuation is ignored in the calculations. Upon finding the theoretical guided wave characteristics, experiments were conducted to see if the aim could be achieved in a realistic scenario. A steel pipe with a diameter of 34 mm and wall thickness of 5.5 mm is considered. High reverberation levels at high frequency propagations due to mode conversion are studied. Having only a limited number of transducers could be a reason for high reverberation at high frequencies.**

Keywords*— *Condition Monitoring, Dispersion, Guided Wave Method, Piezoelectric Elements, Torsional Mode

I. INTRODUCTION

Corrosion is one of the major issues regarding the integrity of assets for a wide range of industries; hence inspections are currently conducted at regular intervals to ensure a sufficient quality of these assets. Obtaining cost reduction while maintaining a high level of reliability and safety of installations is a major challenge. Currently, guided wave technology seems to be the most successful method; however its main applications have been to relatively long and large diameter pipes, i.e., greater than 70 mm [1-3]. In pipes, there are three main ultrasonic guided waves in the axial direction, namely longitudinal, torsional and flexural. These waves propagate along the pipe axially from the excitation area. Reflection of waves from cracks due to different acoustic impedances is processed to find crack sizes and locations. The ability of guided waves to locate cracks and notches including the effect of defect size on the reflected echo has been investigated by many researchers [4-6]. The most recent works such as Demma et. al [6] and Hu [7] have used the axially symmetric T(0,1) mode in 70 mm diameter 5.5 mm thick steel pipes. Most of the previous investigations have studied large pipes with axially symmetric L(0,2) and T(0,1) modes. Mostly, rings of transducers placed with minimum spacing to suppress the unwanted modes have been used to generate only the desired modes. In this paper, the challenges of using the axially symmetric and non-dispersive T(0,1) modes for small diameter pipes were investigated. At the axially symmetric modes, torsional modes are preferred over longitudinal modes because the mode shape of the torsional T(0,1) mode is not frequency dependent. A large advantage of the torsional mode is that it is unaffected by the non-viscous fluid content of the pipe [8]. A torsional mode can detect longitudinal cracks, whereas a longitudinal mode is insensitive to defects parallel to the pipe axis as it does not have radial displacement. However, the range of inspection in longitudinal mode L(0,2) is wider than the respective torsional mode. Also, as torsional modes are sensitive to circumferential changes, if there is a support bracket on the pipe, the reflected signal is strong and hence it is difficult to detect any corrosion on the bracket [8]. In this paper, an incident T(0,1) mode is considered as a complete non-dispersive axially symmetric mode, but mode conversion to the non-symmetric modes happens due to non-axisymmetric defects, as well as the fact that longitudinal and flexural modes (as well as the desired torsional modes) are generated by the transducers.

II. METHODOLOGY

A. Dispersion

The dispersion curves describe the solutions to the modal wave propagation equations which give the properties of the guided wave such as phase velocity, group velocity, energy velocity, attenuation, and mode shape. This information enables the prediction of test results and decision making with regards to selecting the most appropriate guided wave for propagation [9]. From the relationships between stress, strain and displacement the characteristic matrix can be obtained by satisfying the boundary conditions. The coefficient matrix (Equation B16) in Appendix B is set to zero in order to satisfy the nontrivial solution [10]. The characteristic matrix is a

function of thickness, material properties, frequency and wavenumber, introduced as a function of frequency and wavenumber given by the properties of pipe. The roots of this characteristic function, which give the dispersion curves, are found using a numerical root-finding algorithm and the mode shapes are obtained by substituting these roots back into the governing equations. In this work, the roots were extracted by finding the sign changes in the output function using Muller's method. The solution gives the variation in velocity for a mode versus frequency or versus the frequency-thickness product; this product is effectively a normalised frequency.

B. Group and Phase Velocities

Dispersion curves for a group of waves can be different from individual frequency waves, so it is necessary to clarify the concepts of group velocities. The group velocity $\boldsymbol{c_g}$ is the velocity at which a group of waves will travel at a given frequency while the phase velocity is the wave velocity of each individual peaks of a single frequency wave. Phase velocity $\boldsymbol{c_p}$ and group velocity $\boldsymbol{c_g}$ are defined as

$$c_p = \frac{\omega}{k}, \text{ and} \tag{1}$$

$$c_g = \frac{\partial \omega}{\partial k}, \tag{2}$$

where k is the wavenumber. Phase and group velocities are related to each other through

$$c_g = \frac{\partial (c_p k)}{\partial k} = c_p + k\frac{\partial (c_p)}{\partial k}. \tag{3}$$

Here, $c_p = c_p(k)$ expresses the fact that c_p is a function of wavenumber [9].

C. Phase and Group Velocity Dispersion Curves Implementation in MATLAB

The aim of the MATLAB implementation in this paper is to plot the phase and group velocities for a range of frequencies. To do this, the wave number in the characteristic equation for torsional modes needs to be determined. From equation B16 in Appendix B, the determinant of matrix can be considered as:

$$\mathrm{W_n}(\beta \mathrm{r_{in}})\mathrm{Z_n}(\beta \mathrm{r_{ext}}) - \mathrm{Z_n}(\beta \mathrm{r_{in}})\mathrm{W_n}(\beta \mathrm{r_{ext}}) = 0. \tag{4}$$

From the roots β the wavenumber k for real and complex β were found. When β is real, real Bessel functions are used as

$$\mathrm{Y_n}(\beta r_{in})J_\mathrm{n}(\beta r_{ext}) - \mathrm{J_n}(\beta r_{in})\mathrm{Y_n}(\beta r_{ext}) = 0, \tag{5}$$

and for complex β,

$$\mathrm{K_n}(\beta r_{in})I_\mathrm{n}(\beta r_{ext}) - \mathrm{I_n}(\beta r_{in})\mathrm{K_n}(\beta r_{ext}) = 0, \tag{6}$$

which are given in Table B1. Equations (5) and (6) are written as functions of β. The Root Sign Change method is used here as a first step to find the roots of Equations (5) and (6) by finding the sign change intervals in the determinant function as a result of varying β. Muller's method [11] uses these intervals as an initial guess to find a more precise value of β. This specific combination of methods was chosen as a compromise between simplicity and accuracy (required because the determinant function is sensitive to wayward changes in β). Interval sizing for the Sign Change Root Finder method is of critical importance because a grid too coarse may lead to some roots not being identified (resulting in missing values of β) and a grid too fine will result in a script that takes a great amount of time to execute. Through experimentation, the most suitable range and step-size for β values were found to be 0 to 50000 and 100 respectively. The calculated values of wavenumber may be real or complex; real valued wavenumbers correspond to propagating wave modes. The system is assumed to be lossless, so only the real roots are considered, but note that Muller's method can be used to find complex roots as well. Since β values for each torsional mode can be found at each frequency, a value known as the cut-off frequency needs to be identified so that the dispersion curves can be plotted. The cut-off frequency is the frequency at which the phase velocity of a given dispersive mode approaches infinity from a higher frequency value. It is also the value at which the wavenumber is zero. The cut-off frequency can also be defined as

$$\mathrm{f_{Cut-off}} = \frac{\mathrm{c_s}\beta}{2\pi} \tag{7}$$

The group velocity at a point is related to the phase velocity at that point by

$$\mathrm{c_g} = \frac{\partial \omega}{\partial \mathrm{k}} = \frac{\mathrm{k\,c_s}}{\sqrt{\mathrm{k^2}+\beta^2}}. \tag{8}$$

In addition to torsional mode dispersion curves, it is also necessary to find the dispersion curves for longitudinal modes. This is because of the mode conversion which happens between torsional and longitudinal modes. The main difference is that the torsional and longitudinal modes have different characteristic functions. The functions differ also in the fact that a longitudinal mode is a function of frequency, meaning that Muller's method needs to be applied for each frequency value separately. This is cumbersome, so a more time-efficient solution needs to be considered. In this implementation, the determinant of a 4×4 matrix (B16) is calculated for each possible value of k for each frequency separately. The implementation finds the real sign changes in the function, thus finds the values of k that satisfy the characteristic equation. The range and step-size for k values to search through was found through trials, because they can cause the same problems as a poor range choice of step size, as discussed in the previous section. The k values that correspond to the roots are used to find the phase velocity, given by equation (B18). A similar process was applied to the flexural modes. A flexural mode is a non-axially symmetric mode, unlike the longitudinal mode; this difference modifies the determinant of the 4×4 matrix equation (B16). Also, the search domain and step-size for the k values were found through trials, and the chosen step size was reduced since until the missing roots were covered.

III. EXPERIMENTAL SETUP

A function generator (HP 33120A) triggered tone bursts of two cycles with a 10 Hz burst rate and an 18 V peak-peak voltage and a signal amplifier (ORTEC Precision AC Amplifier 9452) with 1 MHz and 100 kHz low pass and high pass filters was used. The system used the through–transmission method, i.e., two identical transducers (a receiver and a transmitter) were used. The input and output signals were digitized by the oscilloscope (LeCroy 9304C) and stored. The oscilloscope was used to average the signal with 300 sweeps in its math function. Data acquisition and processing of the oscilloscope and controlling the oscilloscope were done with MATLAB using GPIB bus.

Frequency bandpass filters including low-pass and high-pass (KROHN-HITE, model: 3202 filter), are very common in signal processing and are also used in several different applications using guided waves [5]. In the experimental work here, a bandpass filter was used to remove some high frequencies when the signals were rectified in order to smooth the signal.

A. Frequency Tuning on the Pipe

Frequency tuning with the axially symmetric mode T(0,1) was performed as an important first step of each experiment [13]. Here, frequency tuning was used to find a frequency that could clearly detect the pipe end and a defect. Tests were carried out on a 34 mm diameter steel pipe with 5.5 mm wall thickness. Tests were performed with one transmitter and one receiver, 100 mm apart, with the transmitter placed 170 mm away from one end of the pipe. Both sensors were placed on the left side of the pipe. When an incident wave is generated with the transducers on the pipe, the echo from the end of the pipe and the direct signal are both expected to arrive at the receiver. Defect responses are frequency-dependent so it is necessary to find the correct frequency in order to detect the defect with maximum amplitude response. Also, high frequency guided waves are utilized when sensitivity to small defects is important. In general, guided waves in the frequency range of 100 - 800 kHz were used to identify defects as small as 0.1% of the pipe's total cross sectional area (CSA). But low frequency guided waves are used for inspecting larger distances where sensitivity to small defects is not a main concern. The frequency range of 20 - 100 kHz can be used to inspect defects as small as 5% of the pipe's CSA [6]. Since this work is concerned specifically with pipes of 34 mm diameters and small size defects (1.7% CSA), higher frequencies are preferable. However, after tests with different frequencies, as shown in Figure 1, it was realized that higher frequencies (higher than 100 kHz) produce stronger reverberations. From these experiments it was found that piezoelectric shear transducers excite longitudinal and flexural modes as well as torsional modes, however in literature the array of elements were attached around the pipe (axially symmetric position recommended) to suppress the non-axially symmetric F(m,n) modes [12]. In the following test three different frequencies, below the first torsional non-dispersive mode (below 350 kHz), were chosen to identify the possible source of this reverberation. It was found that increasing the frequency caused the reverberation to increase.

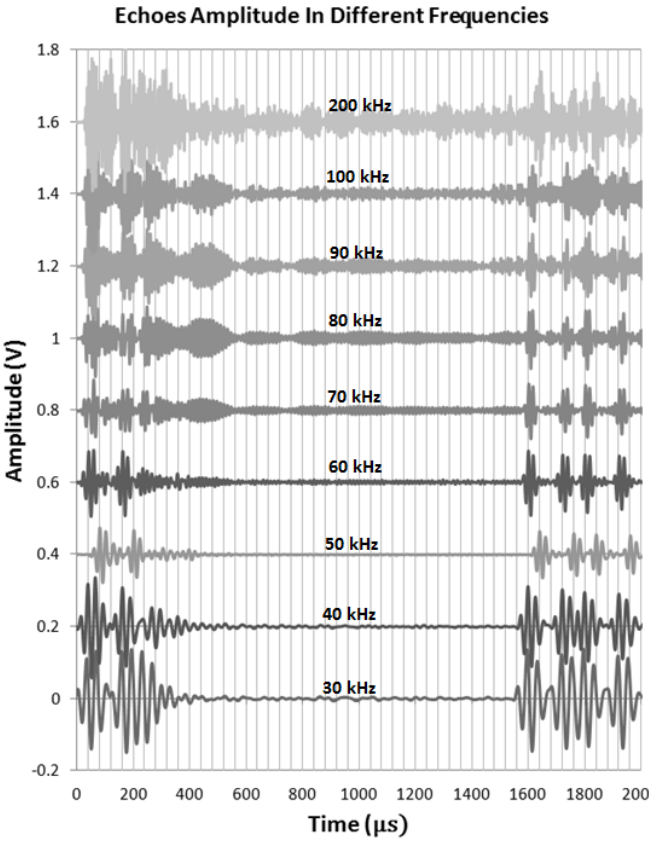

Figure 1. *Amplitude of echoes for different frequencies from 30 - 200 kHz. For each frequency the signal incremented by 0.2V as shown by a different level in this figure. The tests were performed on a 34 mm diameter steel pipe with 5.5 mm wall thickness, with one transmitter and one receiver 100 mm apart, with the transmitter placed 170 mm away from one end of the pipe, and both were placed on the left side of the pipe. The first wave corresponds to the direct arrival, then the pipe end echoes appear between the first end echo and second end echo. The reverberation appeared at a frequency higher than 50 kHz. The tests were performed on a clean pipe without any defects.*

The dispersion graphs in Figure 2, describe the velocity variation of each mode with frequencies, and apply only to the pipe considered in this study. The group velocity dispersion curves were used to find the wave velocity of each mode and consequently the effects of different modes on the received signal reverberation. The dispersion curves in Figure 2 show that modes propagate at 50 - 400 kHz. For example, at 50 kHz, T(0,1), L(0,1), F(1,1), F(1,2), F(2,1) and F(3,1) propagate at different group velocities. The first echo from the pipe end should travel 440 mm, at a group velocity of 3,309 ms^{-1} when T(0,1) is excited, and the echo should have appeared at 133 µs. The other modes that are slower should appear after these two. Having calculated all the modes' travel times, they were compared with the signal

from the receiver (Figure 3) to see how the reverberation compared to the unwanted modes (here longitudinal and flexural). Figure 3 shows the received signal at 50 kHz when one transmitter and one receiver were used, both placed in front of each other (i.e., at 0°). The unwanted modes such as L(0,1) and F(1,2), F(2,1), F(1,1), L(0,1) and F(1,2), F(2,1) and F(1,1) are found to match the unwanted waves.

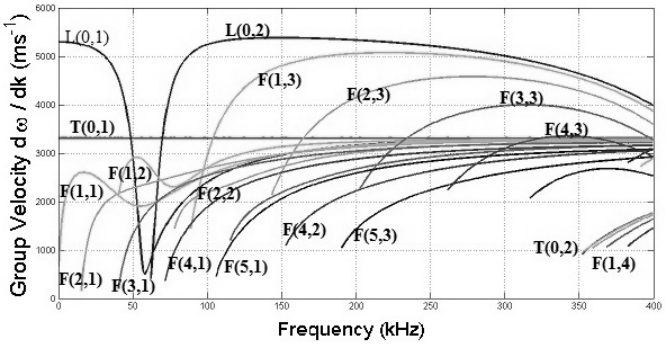

Figure 2. *Group velocity dispersion curves for the steel pipe (Outer diameter: 34 mm, wall thickness: 5.5 mm.).*

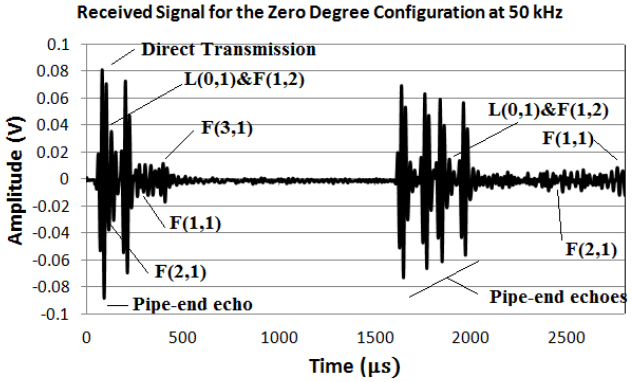

Figure 3. *Received signal for the zero-degree configuration at 50 kHz.*

IV. CONCLUSION

Experimental tests were performed on a steel pipe with a diameter of 34 mm and a wall thickness of 5.5 mm. Increasing the frequency caused an increase in the reverberation level when only two transducers were used. In order to decrease the reverberation level at higher frequencies, increasing the number of receivers and transmitters to suppress the unwanted modes is a method used previously in the literature. A larger number of transducers would help to further this investigation. The reflection from the defect and pipe end has been shown to increase with frequency. To solve these problems (including detection of smaller defects), a larger number of transducers is recommended. For a pipe with 34 mm diameter, it is estimated that eight transducers would be required if the frequency was chose 100 kHz. Hence, the possibility of finding smaller defects by increasing the frequency and the number of transducer can be examined. The effect of losses (due to pipe contents and its underground surroundings) in the pipe system could be accounted for in the MATLAB scripts. The implementation of a two-layered pipe in the MATLAB script could help to expand the scope of research.

APPENDIX A: EQUATION OF MOTION IN ISOTROPIC MEDIA

Wave propagation in unbounded, isotropic media is well documented in many textbooks [9]. The equation of motion for an isotropic elastic medium (without considering body forces), is given by the Navier's equation,

$$(\lambda + 2\mu)\nabla\nabla \cdot \mathrm{u} + \mu\,\nabla^2\mathrm{u} = \rho\left(\frac{\partial^2 \mathrm{u}}{\partial t^2}\right), \qquad \text{(A1)}$$

where u is the three dimensional displacement vector, ρ is the material density, λ and μ are Lame's constants and ∇^2 is the three dimensional Laplace operator. The vector u is expressed by Helmholtz decomposition as the sum of a compressional scalar potential ∅, and equivoluminal vector potential, H according to:

$$\mathrm{u} = \nabla\emptyset + \nabla \times \mathrm{H} \qquad \text{(A2)}$$

$$\text{with } \nabla.\,\mathrm{H} = 0. \qquad \text{(A3)}$$

Substitution of Equation (A2) into Navier's equation (A1) gives

$$c_l{}^2\nabla^2\emptyset = \frac{\partial^2\emptyset}{\partial t^2}, \text{ and} \qquad \text{(A4)}$$

$$c_s{}^2\nabla^2\mathrm{H} = \frac{\partial^2 \mathrm{H}}{\partial t^2}; \qquad \text{(A5)}$$

The displacement equations of motion are satisfied if the potentials ∅ and H satisfy the wave equations. Equation (A4) describes the longitudinal waves and equation (A5) describes the shear waves. c_l and c_s are the longitudinal and shear wave velocities in the infinite isotropic medium, given as:

$$\mathrm{c_l} = \sqrt{\frac{\lambda+2\mu}{\rho}}, \text{ and} \qquad \text{(A6)}$$

$$\mathrm{c_s} = \sqrt{\frac{\mu}{\rho}}. \qquad \text{(A7)}$$

Longitudinal and shear waves are the only types of waves that can propagate in an unbounded isotropic medium and without interaction in the unbounded media (this can be proved from equations A4 and A5). For harmonic waves the scalar potential ∅ and the directional component of vector potential H are defined as

$$\emptyset = \emptyset_0 \mathrm{e}^{\mathrm{i}(k_l.\ z-\omega t)}, \text{ and} \qquad \text{(A8)}$$

$$\mathrm{H} = \mathrm{H}_0 \mathrm{e}^{\mathrm{i}(k_s.\ z-\omega t)}, \qquad \text{(A9)}$$

where k_l and k_s are the longitudinal and shear wave vectors and $\emptyset_0$ and H_0 are initial constants.

APPENDIX B: WAVE PROPAGATION IN A HOLLOW CYLINDER

The geometry of a cylindrical pipe is shown in Figure B1 using the cylindrical coordinate system. For the propagation of waves in a hollow cylinder, the potential ∅ and components of vector potential H can be described as

$$\emptyset = \mathrm{f(r)}\cos(\mathrm{n\theta})\cos(\omega \mathrm{t} + \mathrm{kz}), \quad \text{(B1)}$$
$$\mathrm{H_r} = \mathrm{g_r(r)}\sin(\mathrm{n\theta})\sin(\omega \mathrm{t} + \mathrm{kz}),$$
$$\mathrm{H_\theta} = \mathrm{g_\theta(r)}\cos(\mathrm{n\theta})\sin(\omega \mathrm{t} + \mathrm{kz}) \text{ and}$$
$$\mathrm{H_z} = \mathrm{g_z(r)}\sin(\mathrm{n\theta})\cos(\omega \mathrm{t} + \mathrm{kz})$$

where k is the component of the wave vector in the axial direction and n is the circumferential order. Substitution of (B1) into equations (A8) and (A9) gives the solution for the $\mathrm{f}(r), \mathrm{g}_r(r), \mathrm{g}_\theta(r)$ and $\mathrm{g}_z(r)$ in terms of Bessel functions J and Y and the modified Bessel functions, I and K with arguments of either β or α. β and α can be real or complex and are given by

$$\beta = \sqrt{\frac{\omega^2}{{c_s}^2} - k^2}\text{, and} \quad \text{(B2)}$$

$$\alpha = \sqrt{\frac{\omega^2}{{c_l}^2} - k^2}\,. \quad \text{(B3)}$$

Also, $\beta_1 r = |\beta r|$, and $\alpha_1 r = |\alpha r|$ [9].

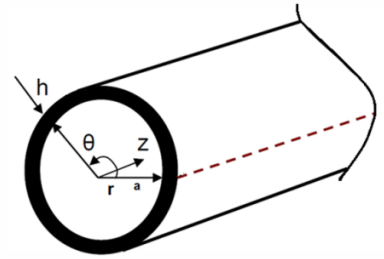

Figure B1. *Schematic of pipe geometry, z is along the pipe, r is radial direction, θ is angle position, a is the internal radius and h is the wall thickness.*

The assumed particle displacement components in the radial (u_r), circumferential (u_θ), and axial (u_z) directions are [B1]

$$\mathrm{u}_r = \mathrm{U_r}(r)\cos(n\theta)\cos(\omega t + kz), \quad \text{(B4)}$$
$$\mathrm{u}_\theta = \mathrm{U}_\theta(r)\sin(n\theta)\cos(\omega t + kz) \text{ and} \quad \text{(B5)}$$
$$\mathrm{u}_z = \mathrm{U}_z(r)\cos(n\theta)\sin(\omega t + kz), \quad \text{(B6)}$$

where $\mathrm{U}_r(r), \mathrm{U}_\theta(r)$ and $\mathrm{U}_z(r)$ are the corresponding displacement amplitudes, composed of Bessel functions or modified Bessel functions depending on the wavenumber characteristic. Differentiation with respect to r yields the strain-displacement in cylindrical coordinates:

$$\varepsilon_{rr} = \frac{\partial \mathrm{u}_r}{\partial r}, \quad \text{(B7)}$$

$$\varepsilon_{r\theta} = \left(\tfrac{1}{2}\right)\left[\mathrm{r}\frac{\partial}{\partial r}\left(\frac{\mathrm{u}_\theta}{r}\right) + \frac{1}{r}\frac{\partial \mathrm{u}_r}{\partial \theta}\right], \text{ and} \quad \text{(B8)}$$

$$\varepsilon_{rz} = \left(\frac{1}{2}\right)\left[r\frac{\partial \mathrm{u}_r}{\partial z} + \frac{1}{r}\frac{\partial \mathrm{u}_z}{\partial \theta}\right]. \quad \text{(B9)}$$

Hooke's Law can be used to define relationships between stresses and strains

$$\sigma_{rr} = \Delta\lambda + 2\mu\varepsilon_{rr}\,, \quad \text{(B10)}$$
$$\sigma_{r\theta} = 2\mu\varepsilon_{r\theta}\text{, and} \quad \text{(B11)}$$
$$\sigma_{rz} = 2\mu\varepsilon_{rz}, \quad \text{(B12)}$$

where $\Delta = \nabla^2\emptyset = -(\alpha^2 + k^2)f\cos(n\theta)\cos(\omega t + kz)$ is dilation. The boundary conditions for the pipe geometry for free motion are given by:

$$\sigma_{rr} = \sigma_{rz} = \sigma_{r\theta} = 0 \text{ at } r = a \text{ and at } r = a{+}h = b \quad \text{(B13)}$$

where a is internal radius, b is the external radius and h is the pipe thickness. Having related strains to small displacements along the pipe, stresses are related to strains to yield the general form of Hooke's Law, so

$$\begin{bmatrix}\sigma_{rr}\\ \sigma_{\theta\theta}\\ \sigma_{zz}\\ \sigma_{\theta z}\\ \sigma_{rz}\\ \sigma_{r\theta}\end{bmatrix} = \begin{bmatrix}\mathrm{C_{11}} & \mathrm{C_{12}} & \mathrm{C_{13}} & \mathrm{C_{14}} & \mathrm{C_{15}} & \mathrm{C_{16}}\\ \mathrm{C_{21}} & \mathrm{C_{22}} & \mathrm{C_{23}} & \mathrm{C_{24}} & \mathrm{C_{25}} & \mathrm{C_{26}}\\ \mathrm{C_{31}} & \mathrm{C_{32}} & \mathrm{C_{33}} & \mathrm{C_{34}} & \mathrm{C_{35}} & \mathrm{C_{36}}\\ \mathrm{C_{41}} & \mathrm{C_{42}} & \mathrm{C_{43}} & \mathrm{C_{44}} & \mathrm{C_{45}} & \mathrm{C_{46}}\\ \mathrm{C_{51}} & \mathrm{C_{52}} & \mathrm{C_{53}} & \mathrm{C_{54}} & \mathrm{C_{55}} & \mathrm{C_{56}}\\ \mathrm{C_{61}} & \mathrm{C_{62}} & \mathrm{C_{63}} & \mathrm{C_{64}} & \mathrm{C_{65}} & \mathrm{C_{66}}\end{bmatrix} \times \begin{bmatrix}L^+\\ L^-\\ SV^+\\ SV^-\\ SH^+\\ SH^-\end{bmatrix} \quad \text{(B14)}$$

where SV is the vertical component of shear deformation, SH is the shear horizontal deformation component and L is the longitudinal deformation component. The positive and negative signs refer to the direction of propagation. The characteristic equation formed by determinant of the Bessel functions is

$$\left|\mathrm{C_{ij}}\right| = 0, (\mathrm{i, j} = 1 \text{ to } 6), \quad \text{(B15)}$$

where i denotes the rows and j the columns of the determinant. Hence, the dispersion characteristic equation for a hollow cylinder is given by [B1]

$$\left[\mathrm{C_{ij}}\right] = \begin{bmatrix}\mathrm{C_{11}} & \mathrm{C_{12}} & \mathrm{C_{13}} & \mathrm{C_{14}} & \mathrm{C_{15}} & \mathrm{C_{16}}\\ \mathrm{C_{21}} & \mathrm{C_{22}} & \mathrm{C_{23}} & \mathrm{C_{24}} & \mathrm{C_{25}} & \mathrm{C_{26}}\\ \mathrm{C_{31}} & \mathrm{C_{32}} & \mathrm{C_{33}} & \mathrm{C_{34}} & \mathrm{C_{35}} & \mathrm{C_{36}}\\ \mathrm{C_{41}} & \mathrm{C_{42}} & \mathrm{C_{43}} & \mathrm{C_{44}} & \mathrm{C_{45}} & \mathrm{C_{46}}\\ \mathrm{C_{51}} & \mathrm{C_{52}} & \mathrm{C_{53}} & \mathrm{C_{54}} & \mathrm{C_{55}} & \mathrm{C_{56}}\\ \mathrm{C_{61}} & \mathrm{C_{62}} & \mathrm{C_{63}} & \mathrm{C_{64}} & \mathrm{C_{65}} & \mathrm{C_{66}}\end{bmatrix} \quad \text{(B16)}$$

$\mathrm{C_{11}} = [2\mathrm{n}(\mathrm{n}-1) - (\beta^2 - k^2){r_{in}}^2]\,\mathrm{Z_n}(\alpha_1 r_{in}) + 2\lambda_1\alpha_1 r_{in}\mathrm{Z_{n+1}}(\alpha_1 r_{in})$,
$\mathrm{C_{12}} = 2k\beta_1 {r_{in}}^2\mathrm{Z_n}(\beta_1 r_{in}) - 2kr_{in}(\mathrm{n}+1)\mathrm{Z_{n+1}}(\beta_1 r_{in})$,
$\mathrm{C_{13}} = -2\mathrm{n}(\mathrm{n}-1)\mathrm{Z_n}(\beta_1 r_{in}) + 2\lambda_2\mathrm{n}\beta_1 r_{in}\mathrm{Z_{n+1}}(\beta_1 r_{in})$,
$\mathrm{C_{14}} = [2\mathrm{n}(\mathrm{n}-1) - (\beta^2 - k^2){r_{in}}^2]\mathrm{W_n}(\alpha_1 r_{in}) + 2\alpha_1 r_{in}\mathrm{W_{n+1}}(\beta_1 r_{in})$,
$\mathrm{C_{15}} = 2\lambda_2 k\beta_1 {r_{in}}^2\mathrm{W_n}(\beta_1 r_{in}) - 2(\mathrm{n}+1)kr_{in}\mathrm{W_{n+1}}(\beta_1 r_{in})$,
$\mathrm{C_{16}} = -2\mathrm{n}(\mathrm{n}-1)\mathrm{W_n}(\beta_1 r_{in}) + 2\mathrm{n}\beta_1 r_{in}\mathrm{W_{n+1}}(\beta_1 r_{in})$,
$\mathrm{C_{21}} = 2\mathrm{n}(\mathrm{n}-1)\mathrm{Z_n}(\alpha_1 r_{in}) - 2\lambda_1\mathrm{n}\alpha_1 r_{in}\mathrm{Z_{n+1}}(\alpha_1 r_{in})$,
$\mathrm{C_{22}} = -k\beta_1 {r_{in}}^2\mathrm{Z_n}(\beta_1 r_{in}) + 2kr_{in}(\mathrm{n}+1)\mathrm{Z_{n+1}}(\beta_1 r_{in})$,
$\mathrm{C_{23}} = -\left[2\mathrm{n}(\mathrm{n}-1) - \beta^2{r_{in}}^2\right]\mathrm{Z_n}(\beta_1 r_{in}) - 2\lambda_2\beta_1 r_{in}\mathrm{Z_{n+1}}(\beta_1 r_{in})$,
$\mathrm{C_{24}} = [2\mathrm{n}(\mathrm{n}-1)]\,\mathrm{W_n}(\alpha_1 r_{in}) - 2\mathrm{n}\alpha_1 r_{in}\mathrm{W_{n+1}}(\alpha_1 r_{in})$,
$\mathrm{C_{25}} = -\lambda_2 k\beta_1\, {r_{in}}^2\mathrm{W_n}(\beta_1 r_{in}) + 2kr_{in}(\mathrm{n}+1)\mathrm{W_{n+1}}(\beta_1 r_{in})$,
$\mathrm{C_{26}} = -\left[2\mathrm{n}(\mathrm{n}-1) - \beta^2{r_{in}}^2\right]\mathrm{W_n}(\beta_1 r_{in}) - 2\beta_1 r_{in}\mathrm{W_{n+1}}(\beta_1 r_{in})$,
$\mathrm{C_{31}} = 2\mathrm{n}k\alpha_1\mathrm{Z_n}(\alpha_1 r_{in}) - 2\lambda_1\alpha_1 kr_{in}{}^2\mathrm{Z_{n+1}}(\alpha_1 r_{in})$,
$\mathrm{C_{32}} = \mathrm{n}\beta_1 r_{in}\mathrm{Z_n}(\beta_1 r_{in}) - (\beta^2 - k^2){r_{in}}^2\mathrm{Z_{n+1}}(\beta_1 r_{in})$,
$\mathrm{C_{33}} = -\mathrm{n}kr_{in}\mathrm{Z_n}(\beta_1 r_{in})$,
$\mathrm{C_{34}} = 2\mathrm{n}kr_{in}\mathrm{W_n}(\alpha_1 r_{in}) - 2k\alpha_1 {r_{in}}^2\mathrm{W_{n+1}}(\alpha_1 r_{in})$,
$\mathrm{C_{35}} = \mathrm{n}\lambda_2\beta_1 r_{in}\mathrm{W_n}(\beta_1 r_{in}) - (\beta^2 - k^2){r_{in}}^2\mathrm{W_{n+1}}(\beta_1 r_{in})$,
$\mathrm{C_{36}} = -\mathrm{n}kr_{in}\mathrm{W_n}(\beta_1 r_{in})$,
$\mathrm{C_{41}} = [2\mathrm{n}(\mathrm{n}-1) - (\beta^2 - k^2){r_{ext}}^2]\,\mathrm{Z_n}(\alpha_1 r_{ext}) + 2\lambda_1\alpha_1 r_{in}\mathrm{Z_{n+1}}(\alpha_1 r_{ext})$,
$\mathrm{C_{42}} = 2k\beta_1 {r_{ext}}^2\mathrm{Z_n}(\beta_1 r_{ext}) - 2kr_{ext}(\mathrm{n}+1)\mathrm{Z_{n+1}}(\beta_1 r_{ext})$,
$\mathrm{C_{43}} = -2\mathrm{n}(\mathrm{n}-1)\mathrm{Z_n}(\beta_1 r_{ext}) + 2\lambda_2\mathrm{n}\beta_1 r_{ext}\mathrm{Z_{n+1}}(\beta_1 r_{ext})$,
$\mathrm{C_{44}} = [2\mathrm{n}(\mathrm{n}-1) - (\beta^2 - k^2){r_{ext}}^2]\mathrm{W_n}(\alpha_1 r_{ext}) + 2\alpha_1 r_{ext}\mathrm{W_{n+1}}(\beta_1 r_{ext})$,
$\mathrm{C_{45}} = 2\lambda_2 k\beta_1 {r_{ext}}^2\mathrm{W_n}(\beta_1 r_{ext}) - 2(\mathrm{n}+1)kr_{ext}\mathrm{W_{n+1}}(\beta_1 r_{ext})$,
$\mathrm{C_{46}} = -2\mathrm{n}(\mathrm{n}-1)\mathrm{W_n}(\beta_1 r_{ext}) + 2\mathrm{n}\beta_1 r_{ext}\mathrm{W_{n+1}}(\beta_1 r_{ext})$,
$\mathrm{C_{51}} = 2\mathrm{n}(\mathrm{n}-1)\mathrm{Z_n}(\alpha_1 r_{ext}) - 2\lambda_1\mathrm{n}\alpha_1 r_{ext}\mathrm{Z_{n+1}}(\alpha_1 r_{ext})$,
$\mathrm{C_{52}} = -k\beta_1 {r_{ext}}^2\mathrm{Z_n}(\beta_1 r_{ext}) + 2kr_{ext}(\mathrm{n}+1)\mathrm{Z_{n+1}}(\beta_1 r_{ext})$,
$\mathrm{C_{53}} = -\left[2\mathrm{n}(\mathrm{n}-1) - \beta^2{r_{ext}}^2\right]\mathrm{Z_n}(\beta_1 r_{ext}) - 2\lambda_2\beta_1 r_{ext}\mathrm{Z_{n+1}}(\beta_1 r_{ext})$,
$\mathrm{C_{54}} = [2\mathrm{n}(\mathrm{n}-1)]\,\mathrm{W_n}(\alpha_1 r_{ext}) - 2\mathrm{n}\alpha_1 b\mathrm{W_{n+1}}(\alpha_1 r_{ext})$,
$\mathrm{C_{55}} = -\lambda_2 k\beta_1\, {r_{ext}}^2\mathrm{W_n}(\beta_1 r_{ext}) + 2kr_{ext}b(\mathrm{n}+1)\mathrm{W_{n+1}}(\beta_1 r_{ext})$,
$\mathrm{C_{56}} = -\left[2\mathrm{n}(\mathrm{n}-1) - \beta^2{r_{ext}}^2\right]\mathrm{W_n}(\beta_1 r_{ext}) - 2\beta_1 b\mathrm{W_{n+1}}(\beta_1 r_{ext})$,
$\mathrm{C_{61}} = 2\mathrm{n}k\alpha_1\mathrm{Z_n}(\alpha_1 r_{ext}) - 2\lambda_1\alpha_1 kr_{ext}{}^2\mathrm{Z_{n+1}}(\alpha_1 r_{ext})$,
$\mathrm{C_{62}} = \mathrm{n}\beta_1 r_{ext}\mathrm{Z_n}(\beta_1 r_{ext}) - (\beta^2 - k^2){r_{ext}}^2\mathrm{Z_{n+1}}(\beta_1 r_{ext})$,
$\mathrm{C_{63}} = -\mathrm{n}kr_{ext}\mathrm{Z_n}(\beta_1 r_{ext})$,
$\mathrm{C_{64}} = 2\mathrm{n}kr_{ext}\mathrm{W_n}(\alpha_1 r_{ext}) - 2k\alpha_1 b^2\mathrm{W_{n+1}}(\alpha_1 r_{ext})$,
$\mathrm{C_{65}} = \mathrm{n}\lambda_2\beta_1 r_{ext}\mathrm{W_n}(\beta_1 r_{ext}) - (\beta^2 - k^2){r_{ext}}^2\mathrm{W_{n+1}}(\beta_1 r_{ext})$, and
$\mathrm{C_{66}} = -\mathrm{n}kr_{ext}\mathrm{W_n}(\beta_1 r_{ext})$.

The terms W_n and Z_n in matrix elements represent the Bessel functions with type depending on the value of n. Table B1 shows the appropriate selection of the Bessel functions for selected wave characteristics. As previously mentioned, *n* is the circumferential order of guided waves in a hollow cylinder. n is equal to zero when the modes are axially symmetric. It can change as θ varies but it remains axially symmetric. For axially symmetric modes the frequency equation can be decomposed into the product of two sub determinants with

$$D_1 \cdot D_2 = 0, \tag{B17}$$

where

$$D_1 = \begin{bmatrix} C_{11} & C_{12} & C_{14} & C_{15} \\ C_{31} & C_{32} & C_{34} & C_{35} \\ C_{41} & C_{42} & C_{44} & C_{45} \\ C_{61} & C_{62} & C_{64} & C_{65} \end{bmatrix}, D_2 = \begin{bmatrix} C_{23} & C_{26} \\ C_{53} & C_{56} \end{bmatrix} \tag{B18}$$

Wave-number	Frequency range	Coefficient	Bessel Functions
Real	$\frac{w}{k} < C_l, C_s$	$\beta^2, \alpha^2 < 0$ $\lambda_1 = \lambda_2 = -1$	$Z_n(\alpha r) = I_n(\alpha r)$ $W_n(\alpha r) = K_n(\alpha r)$ $Z_n(\beta r) = I_n(\beta r)$ $Z_n(\beta r) = K_n(\beta r)$
Real	$C_s < \frac{w}{k} < C_l$	$\alpha^2 < 0$ $\beta^2 > 0$ $\lambda_1 = -1$ $\lambda_2 = 1$	$Z_n(\alpha r) = I_n(\alpha r)$ $W_n(\alpha r) = K_n(\alpha r)$ $Z_n(\beta r) = J_n(\beta r)$ $Z_n(\beta r) = Y_n(\beta r)$
Real	$\frac{w}{k} > C_l, C_s$	$\beta^2, \alpha^2 > 0$ $\lambda_1 = \lambda_2 = 1$	$Z_n(\alpha r) = J_n(\alpha r)$ $W_n(\alpha r) = Y_n(\alpha r)$ $Z_n(\beta r) = J_n(\beta r)$ $Z_n(\beta r) = Y_n(\beta r)$
Imaginary	any		
Complex	any	β^2, α^2Complex $\lambda_1, \lambda_2 = 1$	

Table B1. *Bessel function coefficients used for different values of the frequency range: corresponding values of $\lambda_1, \lambda_2, \alpha$ and β in terms of wavenumbers. (λ_1 and λ_2 are weighting coefficients, $_n$ and K_n are complex Bessel functions and J_n and Y_n are real Bessel functions).*

ACKNOWLEDGMENT

The authors would like to thank Mr. Mark Vousden for his valuable suggestions to improve the quality of the paper and his contributions to the numerical simulation.

REFERENCES

[1] A. Volker, A. Mast, J. Bloom, "Experimental results of guided wave travel time topography," AIP Conf. Proc. Vol. 1211, 2010.

[2] L.J. Breon, J.K. Van Velsor, J.L. Rose, "Guided wave damage detection tomography for structural health monitoring in critical zones of pipelines," Mater. Eval, Vol. 65, no. 12, pp. 1215-1219, 2007.

[3] J.M. Liu, C.E. Davis, T.M. Regin, and J. Brophy, "Monitoring the growth of hidden corrosion discontinuities in a pipeline with complex geometry using torsional mode ultrasonic guided wave," Materials Evaluation, Vol. 69, pp. 393-400, 2011.

[4] J.J. Ditri, "Utilization of guided elastic waves for the characterization of circumferential cracks in hollow cylinders, " J. Acoust. Soc. Am. Vol. 96, pp. 3769-3775, 1994c.

[5] D.N. Alleyne, P. Cawley, "Long range propagation of Lamb waves in chemical plant pipework," Materials Evaluation, Vol. 55, pp. 504-508, ISSN:0025-5327, 1997.

[6] A. Demma, P. Cawley, M. Lowe and A. G. Roosenbrand, "The reflection of the fundamental torsional mode from cracks and notches in pipes, " J. Acoust. Soc. Am. 114, Issue 2. pp. 611-625, 2003.

[7] X. Hu, X. Feng and J. Zhou, "Reflection characteristics of guided wave in a pipe with a circumferential crack," The 6th International Workshop on Advanced Smart Materials and Smart Structures Technology, China, 2011.

[8] D.N. Alleyne, B.Pavlakovic, M. Lowe and P. Cawley, "Rapid long range inspection of chemical plant pipework using guided waves," Insight, Vol. 43, pp. 93-96,101, 2001.

[9] J.L. Rose, Ultrasonic waves in solid media, Cambridge University Press, 1999.

[10] D.C. Gazis, "Three dimensional investigation of propagation of waves in hollow circular cylinders. I. Analytical foundation." J. Acoust. Soc. Am. Vol. 31, pp. 568-578, 1959.

[11] W.R. Mekwi, "Iterative Methods for Roots of Polynomials," Ph.D. dissertation, Exeter. College, University of Oxford, 2001.

[12] D. N. Alleyne, P. Cawley, "The excitation of Lamb waves in pipes using dry-coupled piezoelectric transducers, Journal of Nondestructive Evaluation," Vol. 15, pp. 11–20, ISSN:0195-9298, 1996.

[13] Z. Liu, C. He, B. Wu, X. Wang, and S. Yang, "Circumferential and longitudinal defect detection using T(0,1) mode excited by thickness shear mode piezoelectric elements," Ultrasonics.Vol, 44, e1135–e1138,2006.